A Single-Step Method for Accelerometer and Magnetometer Axes Alignment

Paul P. Sotiriadis, *Senior Member, IEEE*, and Konstantinos Papafotis, *Graduate Student Member, IEEE*

***Abstract*— In this work, we introduce a single-step method for axes alignment of a three-axis accelerometer and a three-axis magnetometer. The proposed method is based on the magnetic inclination to derive the inclination angle and the axes alignment rotation matrix, both in closed form. It is applied when the two sensors are fixed on the same rigid platform and requires no special piece of equipment. In contrast to the existing algorithms, it does not rely on an iterative optimization or estimation method; instead, it is executed in a single step. It is two orders of magnitude faster than the existing iterative algorithms based on the same principle. Multiple measurement sets are used to demonstrate the algorithm's computational efficiency, while its accuracy is evaluated through a series of simulated measurements.**

***Index Terms*— Accelerometer, axes alignment, inclination, inertial sensors, magnetometer.**

I. Introduction

THE advancement of microelectromechanical (MEMS) sensors over the past decades significantly reduced the size and cost of accelerometers enabling their wider use. Along with magnetometers, they are nowadays considered a key component of several commercial electronic devices, such as smartphones, activity trackers, alarm systems, and others. The two sensors are commonly combined in several applications, including navigation [1], attitude estimation [2], and human motion tracking [3].

In such cases, except for the individual calibration of the accelerometer and the magnetometer, an extra procedure to align the sensitivity axes of the two sensors is required. The misalignment between the sensors' axes is caused by the misalignment of the sensing element of each sensor with its package, the mutual misalignment of the sensors' packages, and the soft-iron distortion of the magnetometer [4]. It is more evident when the two sensors are in different packages, but it is present even when they are built into the same chip.

Manuscript received March 18, 2020; accepted June 29, 2020. Date of publication July 20, 2020; date of current version December 14, 2020. This work was supported by Greece and the European Union [European Social Fund (ESF)] through the Operational Programme "Human Resources Development, Education and Lifelong Learning" in the context of the project "Strengthening Human Resources Research Potential via Doctorate Research" implemented by the State Scholarships Foundation (IKY) under Grant MIS-5000432. The Associate Editor coordinating the review process was Bruno Ando. *(Corresponding author: Konstantinos Papafotis.)*

The authors are with the Department of Electrical and Computer Engineering, National Technical University of Athens, 15780 Athens, Greece (e-mail: k.papafotis@gmail.com).

Digital Object Identifier 10.1109/TIM.2020.3010387

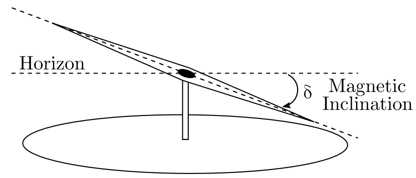

Fig. 1. Magnetic inclination.

In many cases, the axes alignment of the two sensors is part of the calibration procedure, whereas in other ones, it is done separately. Wu *et al.* [5], Kok *et al.* [6], and Kok and Schön [7] proposed a magnetometer calibration algorithm incorporating the axes alignment step. In [4] and [8], the axes alignment is a part of an inertial (accelerometer and gyroscope) and magnetic sensors' calibration algorithm. An accelerometer–magnetometer calibration algorithm also accounting for the axes misalignment is proposed in [9]–[11]. Note that in [5], [6], [10], and [11], the calibration and axes alignment are fused together and cannot be done separately, whereas in [4], [8], and [9], the alignment step is a discrete part of the calibration algorithm.

While many different algorithms for axes alignment have been proposed, most of them are based on two fundamental approaches. The first one (see [5], [7], [8]) is to use a calibrated gyroscope, as reference, to align the axes of a magnetometer with those of an accelerometer and a gyroscope. The second (see [4], [6]) is to exploit the magnetic inclination phenomenon and use the measurements of the two sensors to align their axes. It should be noticed that the second approach does not require any piece of equipment, whereas for the first one, a calibrated gyroscope is required.

Magnetic inclination (or magnetic dip) is the angle between the horizon and the Earth's magnetic field lines, as shown in Fig. 1. It varies with location and time, and it is defined as the normalized inner product of the gravity and the magnetic field.[1]

$$\sin(\delta) = \frac{g^T m}{\|g\|\|m\|}. \tag{1}$$

When the magnetic inclination is exploited, the axes alignment is formulated as an optimization problem, which is usually solved using gradient descent [4] or Newton–Raphson's [9] methods. Both approaches come with a disadvantage; their

[1] All norms in this article are Euclidean norms unless it is indicated otherwise.

solution is given in an iterative way. This implies a significant computational burden and potential convergence issues.

In this work, we derive a closed-form solution for axes alignment of a three-axis accelerometer and a three-axis magnetometer. The proposed method calculates the rotation matrix that maps the magnetometer's axes into the accelerometer's ones, in a single step, without using any iterative optimization (e.g., Newton–Raphson and gradient descent) or estimation (e.g., Kalman filter) algorithm. It applies when the two sensors are fixed on the same rigid platform and are individually calibrated. The evaluation of the proposed method is done through a series of both real and simulated measurements. To this end, we use the 12-step sequence of approximate platform's placements introduced in [4] and no special piece of equipment.

The rest of this article is organized as follows. In Section II, the problem of axes alignment is stated. The proposed method is described in Section III. The method's evaluation using experimental data is presented in Section IV. A variation of the proposed algorithm with improved accuracy is described in Section V. Finally, conclusions are drawn in Section VI.

II. Problem Statement

Consider a three-axis accelerometer and a three-axis magnetometer, both fixed on the same rigid platform, and denote their coordinate frames as $\{A\}$ and $\{M\}$, respectively.

Now, suppose that accelerometer's measurement g_k^A and magnetometer's measurement m_k^M are taken simultaneously when the rigid platform is still (only gravitational acceleration), for $k = 1, 2, \dots, K$ with $K \geq 9$. Platform's orientation changes with k and every measured vector is expressed in the coordinate frame of the corresponding sensor.

Let the gravity vector g and magnetic field m be expressed in a fixed inertial coordinate frame[2] $\{I\}$. For every $k = 1, 2, \dots, K$, there is a rotation matrix $Q_k \in SO(3)$ transforming vectors from the $\{I\}$-frame to the $\{A\}$-frame. Then, the gravity and magnetic field vectors expressed in the $\{A\}$-frame are written as

$$g_k^A = Q_k g \quad \text{and} \quad m_k^A = Q_k m \tag{2}$$

for $k = 1, 2, \dots, K$, respectively. Solving (2) for g and m and replacing them in (1)

$$\sin(\delta) = \frac{\left(g_k^A\right)^T Q_k Q_k^T m_k^A}{\left\| Q_k^T g_k^A \right\| \left\| Q_k^T m_k^A \right\|} = \frac{\left(g_k^A\right)^T m_k^A}{\left\| g_k^A \right\| \left\| m_k^A \right\|} \tag{3}$$

for $k = 1, 2, \dots, K$, where we exploited the orthogonality of Q_k and the rotational invariance of the Euclidean norm.

In (3), the accelerometer's measurement g_k^A is known. The measured magnetic field m_k^M, however, is naturally expressed in the $\{M\}$-frame, and therefore, we need to transform it to the $\{A\}$-frame. To this end, let $R_M^A \in SO(3)$ be the transformation matrix from the $\{M\}$-frame to the $\{A\}$-frame, and then

$$m_k^A = R_M^A m_k^M, \quad k = 1, 2, \dots, K. \tag{4}$$

[2]All coordinate frames are considered to be right-handed.

Combining (3) and (4) and using again the rotational invariance of the Euclidean norm, we get that

$$\sin(\delta) = \frac{\left(g_k^A\right)^T R_M^A m_k^M}{\left\| g_k^A \right\| \left\| m_k^M \right\|}, \quad k = 1, 2, \dots, K. \tag{5}$$

In (5), g_k^A and m_k^M are the known accelerometer's and magnetometer's measurements, respectively, while both R_M^A and inclination angle, δ, are unknown. A standard approach to derive them is to form and solve the optimization problem

$$\begin{aligned} \min_{R_M^A, \delta} \; & \sum_{k=1}^{K} \left(\sin(\delta) - \frac{\left(g_k^A\right)^T R_M^A m_k^M}{\left\| g_k^A \right\| \left\| m_k^M \right\|} \right)^2 \\ \text{s.t.} \; & R_M^A \in SO(3) \\ & \delta \in \left[-\frac{\pi}{2}, \frac{\pi}{2} \right]. \end{aligned} \tag{6}$$

Solving (6) is typically done using either the gradient descent or the Newton–Raphson methods (see [4], [9]). Both are computational costly; gradient descent typically requires hundreds of iterations to converge, whereas Newton–Raphson, although it converges faster, it requires the calculation of the Hessian matrix.

III. Proposed Method

In this work, instead of applying an iterative algorithm to solve (6), we propose a single-step method for calculating R_M^A and δ. The proposed method provides a closed-form solution resulting in significantly improved computational efficiency.

A. Method Description

For the rest of this article, and without loss of generality we assume that the measured gravity and magnetic field vectors are normalized, i.e., $\|g_k^A\| = \|m_k^M\| = 1$ for $k = 1, 2, \dots, K$, and we also set

$$s_\delta \triangleq \sin(\delta).$$

Furthermore, for notational simplicity, we drop the subscript and superscript from R_M^A, i.e., $R \equiv R_M^A$.

To keep the analysis simple, we proceed assuming perfect measurements and deal with the nonidealities of the real ones when it is mandated.

Using identity $\text{vec}(AXB) = (B^T \otimes A)\text{vec}(X)$ [12], where $\otimes$ is Kronecker's product, and the unit magnitude assumption, from (5), we get

$$s_\delta = \left(m_k^M \otimes g_k^A\right)^T \text{vec}(R) \tag{7}$$

for $k = 1, 2, \dots, K$. Then, we express (7) in matrix form as

$$s_\delta \, \underline{1} = A \; \text{vec}(R) \tag{8}$$

where $\underline{1}$ is the $K \times 1$ vector of ones and A is the following $K \times 9$ matrix:

$$A = \begin{bmatrix} \left(m_1^M \otimes g_1^A\right)^T \\ \left(m_2^M \otimes g_2^A\right)^T \\ \vdots \\ \left(m_K^M \otimes g_K^A\right)^T \end{bmatrix}. \tag{9}$$

To proceed, we assume that the measurements are such that A is of full rank, i.e., $\text{rank}(A) = 9$ (see Section III-B). This along with the fact that $\text{vec}(R) \neq 0$, since $R \in SO(3)$, and (8) imply that

$$s_\delta \neq 0. \tag{10}$$

We solve (8) (in the least squares sense [13])[3] to derive

$$\text{vec}(R) = s_\delta (A^T A)^{-1} A^T \underline{1} \tag{11}$$

where the equation is approximate when the measurements are real. Next, we split the 9×1 vector $(A^T A)^{-1} A^T \underline{1}$ into three 3×1 vectors h_1, h_2, and h_3 as

$$(A^T A)^{-1} A^T \underline{1} = \begin{bmatrix} h_1^T & h_2^T & h_3^T \end{bmatrix}^T. \tag{12}$$

Defining matrix H as

$$H = [h_1 \quad h_2 \quad h_3] \tag{13}$$

and using (11)–(13) we express matrix R as

$$R = s_\delta H. \tag{14}$$

Note that in (14), matrix H is known, but s_δ is not. To calculate s_δ, we use the fact that $R \in SO(3)$ and so $\det(R) = 1$ which combined with (14) gives $\det(H) \neq 0$ and

$$1 = {s_\delta}^3 \det(H) \tag{15}$$

and so

$$s_\delta = \frac{1}{\sqrt[3]{\det(H)}} \tag{16}$$

where the cubic root is constrained in the real numbers.

Although (16) is a compact expression, it is not as accurate with real data as the one we derive from the fact that $\|R\|_F = \sqrt{3}$ for $R \in SO(3)$ [12]. Combining it with (14) implies

$$|s_\delta| = \frac{\sqrt{3}}{\|H\|_F} \tag{17}$$

and the sign of s_δ can be recovered from (15) as

$$\text{sgn}(s_\delta) = \text{sgn}(\det(H)). \tag{18}$$

Consider a singular value decomposition (SVD) of matrix H, i.e., $H = U \Sigma V^T$, where $U, V \in O(3)$ and Σ is the diagonal matrix $\Sigma = \text{diag}(\sigma_1, \sigma_2, \sigma_3)$, with $\sigma_1 \geq \sigma_2 \geq \sigma_3 > 0$ since $\det(H) \neq 0$. It is $\|H\|_F = (\sigma_1^2 + \sigma_2^2 + \sigma_3^2)^{1/2}$ [12], which combined with (17) and (18) gives

$$s_\delta = \text{sgn}(\det(H)) \sqrt{\frac{3}{\sigma_1^2 + \sigma_2^2 + \sigma_3^2}}. \tag{19}$$

By substituting (19) into (14), we get R, which ideally belongs to $SO(3)$. When using real measurements, however, R may be close to but not necessarily in $SO(3)$. Thus, instead of R, we derive and use the nearest special orthogonal matrix $\hat{R} \in SO(3)$ to $R = s_\delta H$ defined as the solution of the optimization problem

$$\hat{R} \triangleq \underset{Q \in SO(3)}{\text{argmin}} \|R - Q\|_F.^4 \tag{20}$$

[3]With real measurements, (7) is approximate and (8) is considered as a least-squares problem with solution (11), where R is expected to be close to but not necessarily in $SO(3)$.

[4]$\|X\|_F = (\text{tr}(X^* X))^{1/2}$, $X \in \mathbb{C}^{n \times m}$.

Algorithm 1 Proposed Method

1: Use normalized g_k^A and m_k^M to form matrix A in (9)
2: Verify that A is of full rank
3: Form matrix H in (13) using (12)
4: Derive an SVD, $H = U \Sigma V^T$, $\Sigma = \text{diag}(\sigma_1, \sigma_2, \sigma_3)$
5: Verify that $\sigma_3 > 0$
6: Derive s_δ from (19)
7: Derive $\hat{R}$ from (22)

Even with real measurements, we expect that $\det(R) > 0$, which guarantees the uniqueness of the solution of the orthogonal Procrustes problem [14] in $O(3)$

$$\bar{R} = \underset{Q \in O(3)}{\text{argmin}} \|R - Q\|_F. \tag{21}$$

The solution of (21) is $\bar{R} = \text{sgn}(s_\delta) U V^T$ [14]. It can be derived using the previously calculated SVD of H leading to an SVD of $R = (\text{sgn}(s_\delta) U)(|s_\delta| \Sigma) V^T$ via (14).

Also, note that $\text{sgn}(\det(H)) = \text{sgn}(\det(U V^T))$ which along with (14) and (19) imply that $\det(\bar{R}) = 1$, and therefore, $\hat{R} = \bar{R} \in SO(3)$ is the unique solution of (20), i.e.,

$$\hat{R} = \text{sgn}(\det(H)) U V^T. \tag{22}$$

The proposed method is summarized in Algorithm 1.

An alternative expression of (22) is $\hat{R} = \pm R (R^T R)^{-1/2}$ where the square root is positive definite and the sign such that $\det(R) = 1$. Finally, note that the presented approach to derive s_δ and $\hat{R}$ was selected due to its robust behavior when applied to real measurements. Alternate approaches are briefly mentioned in the Appendix.

B. Measurements Acquisition Procedure

The proposed method aligns the axes of a three-axis accelerometer and a three-axis magnetometer. To this purpose, one can consider the 12-step measurement acquisition procedure in Fig. 2 [4]. The (X, Y, Z) coordinate system in Fig. 2 denotes the platform's body frame (or the accelerometer's $\{A\}$-frame), whereas the $(\tilde{X}, \tilde{Y}, \tilde{Z})$ is the inertial coordinate $\{I\}$-frame. The respective g_k^A and m_k^M, $k = 1, 2, \ldots, 12$, are measured, while the platform is still in each orientation.

Note that the orientations of the sensors' platform in Fig. 2 are meant to be approximate, and no accuracy is needed. Orientation and placement of the sensor can be done by hand with an accuracy of about $\pm 15°$ Euler degrees.

IV. Algorithm's Evaluation

In order to evaluate the convergence and the computational efficiency of the proposed algorithm, we performed a series of experimental measurements. In addition, simulated measurements were used to demonstrate the algorithm's accuracy.

A. Algorithm's Convergence and Computational Efficiency

A series of experimental measurements following the procedure described in Section III-B was performed. Using them, we compare the performance of the proposed algorithm to that

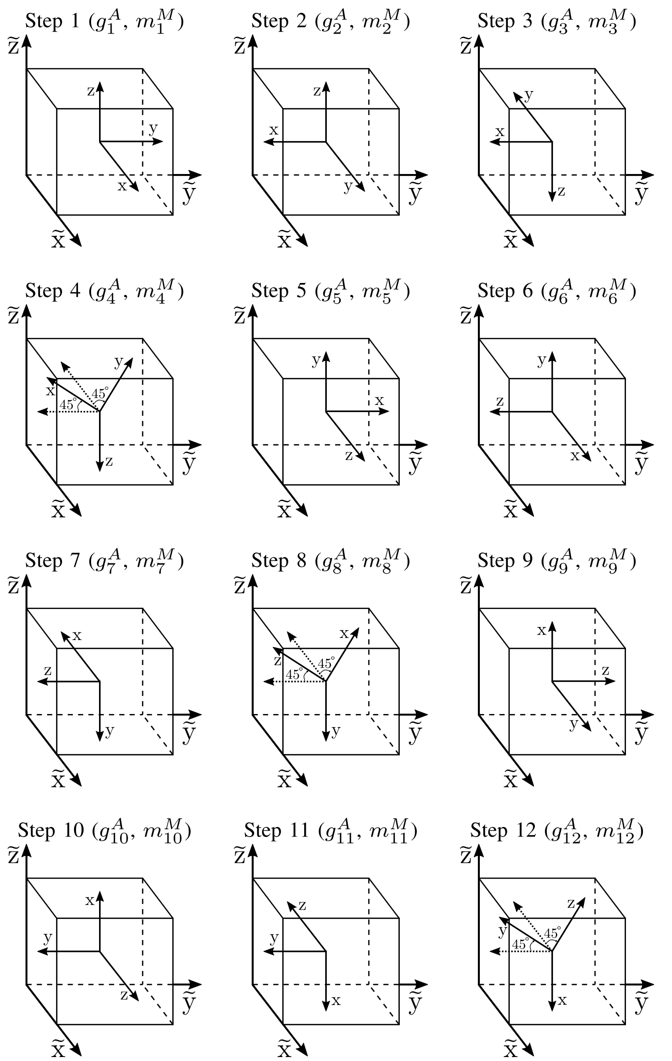

Fig. 2. Recommended sequence of approximate orientations.

TABLE I

MET OF THE PROPOSED ALGORITHM FOR 400 RUNS COMPARED TO THE MET OF NEWTON–RAPHSON AND GRADIENT DESCENT-BASED METHODS

Method	**MET (ms)**	**Relative Time**
Proposed	0.31	×1
Newton-Raphson	54.61	×175
Gradient Descent	84.22	×270

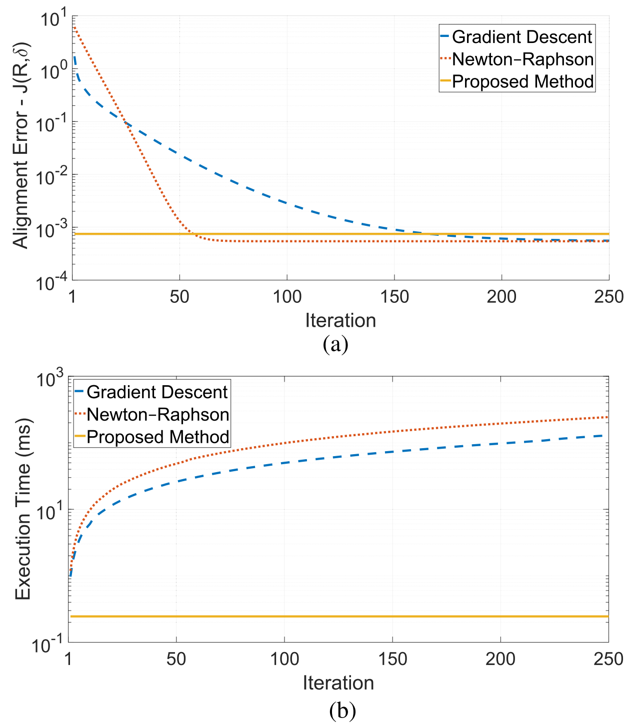

Fig. 3. Performance comparison between the proposed method and the standard iterative methods. (a) Alignment error of the proposed single-step method compared with the alignment error of the gradient descent and Newton–Raphson solutions. The alignment error is evaluated in every iteration step using $J(R, \delta)$ as in (23). (b) Execution time of the proposed single-step method compared with the execution time of the gradient descent and Newton–Raphson solutions parameterized on their iteration step.

of the two popular iterative ones, based on the gradient descent and the Newton–Raphson methods to solve (6).

As a metric of the alignment error, we use the following cost plus penalty function, associated with (6), which also captures the nonorthogonality of matrix R:

$$J(R, \delta) = \sum_{k=1}^{K} \left(\sin(\delta) - \frac{(g_k^A)^T R m_k^M}{\|g_k^A\| \|m_k^M\|} \right)^2 + \|RR^T - I\|_F^2. \tag{23}$$

Note that in our method, the resulting matrix $\hat{R}$ is always in $SO(3)$, and thus, the second term, $\|\hat{R}\hat{R}^T - I\|_F^2$, in (23) is always zero. For the existing methods, however, this is not necessarily the case and this is why the second term is included.

In Fig. 3(a), the alignment error of the proposed method is compared to those of the gradient descent and the Newton–Raphson-based methods. Fig. 3(b) shows the execution time of the three methods as a function of the iteration number.

The proposed method achieves an alignment error of about 7.4×10^{-4} in a total execution time of about 0.3 ms. Newton–Raphson achieves the same alignment error after 57 iterations and about 55 ms; it converges to a slightly smaller alignment error (about 5.5×10^{-4}) after about 80 iterations. Gradient descent method requires 165 iterations and about 80 ms to achieve the proposed method's alignment error, while it also converges to a slightly smaller error (about 5.5×10^{-4}) after about 230 iterations.

The execution time of the three approaches was measured for a total of 400 runs using four different data sets. Gradient descent and Newton–Raphson iterations were terminated when they reached the proposed method's accuracy. The mean execution time (MET) of each of them is presented in Table I. The proposed algorithm is about 175 times faster than Newton–Raphson and 270 times faster than gradient descent. All three algorithms were executed in MATLAB running on a typical quad-core, 8-GB RAM PC.

TABLE II

MEAN VALUE AND VARIANCE OF THE EULER ANGLE REPRESENTATION OF THE RESIDUAL ALIGNMENT ERROR MATRIX E FOR FIVE DIFFERENT ROTATION MATRICES USING THE PROPOSED ALGORITHM

R_A^M $[\psi \ \ \theta \ \ \phi]$	Sensors' Noise σ_g^2, σ_m^2	μ_E $[\mu_{E\psi} \ \ \mu_{E\theta} \ \ \mu_{E\phi}]$	σ_E^2 $[\sigma_{E\psi}^2 \ \ \sigma_{E\theta}^2 \ \ \sigma_{E\phi}^2]$
$[1° \ \ 1° \ \ 1°]$	$5.2 \cdot 10^{-4}$, $5.5 \cdot 10^{-6}$	$[0.001° \ \ 0.002° \ \ -0.002°]$	$[0.017° \ \ 0.012° \ \ 0.015°]$
$[3° \ \ 4° \ \ 5°]$	$5.2 \cdot 10^{-4}$, $5.5 \cdot 10^{-6}$	$[0.003° \ \ -0.001° \ \ 0.003°]$	$[0.031° \ \ 0.017° \ \ 0.024°]$
$[15° \ \ 20° \ \ 25°]$	$5.2 \cdot 10^{-4}$, $5.5 \cdot 10^{-6}$	$[0.005° \ \ 0.001° \ \ -0.002°]$	$[0.021° \ \ 0.025° \ \ 0.009°]$
$[45° \ \ 45° \ \ 45°]$	$5.2 \cdot 10^{-4}$, $5.5 \cdot 10^{-6}$	$[-0.005° \ \ -0.002° \ \ -0.001°]$	$[0.017° \ \ 0.013° \ \ 0.012°]$
$[90° \ \ 0° \ \ 0°]$	$5.2 \cdot 10^{-4}$, $5.5 \cdot 10^{-6}$	$[0.005° \ \ -0.003° \ \ 0.002°]$	$[0.025° \ \ 0.023° \ \ 0.009°]$

In all five cases, noisy simulated measurements were used. The algorithm was run 1000 times for every rotation matrix using different (random) initial gravity g_1^A and magnetic field m_1^A vectors, as well as, different sequences of additive noise. The variances of the additive accelerometer's and magnetometer's noise, σ_g^2 and σ_m^2, respectively, were the same for all datasets.

TABLE III

MEAN VALUE AND VARIANCE OF THE EULER ANGLE REPRESENTATION OF THE RESIDUAL ALIGNMENT ERROR MATRIX E FOR FIVE DIFFERENT ROTATION MATRICES USING THE PROPOSED ALGORITHM'S VARIATION

R_A^M $[\psi \ \ \theta \ \ \phi]$	Sensors' Noise σ_g^2, σ_m^2	μ_E $[\mu_{E\psi} \ \ \mu_{E\theta} \ \ \mu_{E\phi}]$	σ_E^2 $[\sigma_{E\psi}^2 \ \ \sigma_{E\theta}^2 \ \ \sigma_{E\phi}^2]$
$[1° \ \ 1° \ \ 1°]$	$5.2 \cdot 10^{-4}$, $5.5 \cdot 10^{-6}$	$[0.001° \ \ -0.002° \ \ 0.001°]$	$[0.013° \ \ 0.009° \ \ 0.014°]$
$[3° \ \ 4° \ \ 5°]$	$5.2 \cdot 10^{-4}$, $5.5 \cdot 10^{-6}$	$[0.005° \ \ 0.001° \ \ 0.002°]$	$[0.022° \ \ 0.019° \ \ 0.016°]$
$[15° \ \ 20° \ \ 25°]$	$5.2 \cdot 10^{-4}$, $5.5 \cdot 10^{-6}$	$[0.003° \ \ 0.002° \ \ 0.004°]$	$[0.018° \ \ 0.025° \ \ 0.005°]$
$[45° \ \ 45° \ \ 45°]$	$5.2 \cdot 10^{-4}$, $5.5 \cdot 10^{-6}$	$[0.003° \ \ -0.001° \ \ -0.001°]$	$[0.011° \ \ 0.012° \ \ 0.009°]$
$[90° \ \ 0° \ \ 0°]$	$5.2 \cdot 10^{-4}$, $5.5 \cdot 10^{-6}$	$[-0.002° \ \ -0.001° \ \ 0.004°]$	$[0.021° \ \ 0.019° \ \ 0.012°]$

In all five cases, noisy simulated measurements were used. The algorithm was run 1000 times for every rotation matrix using different (random) initial gravity g_1^A and magnetic field m_1^A vectors, as well as, different sequences of additive noise. The variances of the additive accelerometer's and magnetometer's noise, σ_g^2 and σ_m^2, respectively, were the same for all datasets.

B. Algorithm's Accuracy

Recorded measurements are appropriate to demonstrate the convergence and the computational efficiency of the proposed algorithm as they incorporate the nonidealities of a real-world application, e.g., noise, quantization, and residual calibration errors of the accelerometer and the magnetometer. On the other hand, the misalignment of the two sensors is not known, and thus, the algorithm's accuracy cannot be evaluated using recorded measurements. To this purpose, we used both ideal (noiseless) and noisy simulated accelerometer's and magnetometer's measurements.

Simulated measurements were generated following the measurement acquisition procedure mentioned in Section III-B. More specifically, two random unit vectors representing the gravity g_1^A and the magnetic field m_1^A vectors, expressed in the $\{A\}$-frame, were first generated. Then, they were both rotated 11 times according to Fig. 2, resulting in the $\{A\}$-frame measurement vectors g_k^A and m_k^A, $k = 2, 3, \ldots, 12$. The magnetometers' simulated measurements were rotated once more using the selected rotation matrix R_A^M to get the corresponding $\{M\}$-frame measurement vectors m_k^M, $k = 1, 2, \ldots, 12$. Finally, band-limited white noise was added to the measurements. The noise characteristics were chosen to match those of the measurement platform used for the experimental measurements.

Using five different rotation matrices R_A^M, we generated 1000 noiseless and 1000 noisy data sets for every rotation matrix. In every data set, we used different (random) initial gravity g_1^A and magnetic field m_1^A vectors as well as different sequences of additive noise.

We define the residual alignment error matrix E as the product of the original rotation of the $\{M\}$-frame R_A^M with the derived rotation matrix $\hat{R}$, i.e.,

$$E = R_A^M \hat{R}. \tag{24}$$

In the ideal case, where $\hat{R} = R_M^A \equiv (R_A^M)^T$, the error E is equal to the identity matrix, implying zero rotation between the two frames.

Applying the proposed algorithm using the noiseless data sets leads to perfect alignment between the sensors' coordinate frames, i.e., $E = I$ for every data set. When the more realistic noisy measurements were used, a small residual alignment error was observed. The mean value μ_E and the variance σ_E^2 of the Euler angle representation of E for every selected rotation matrix are presented in Table II.

V. IMPROVED-ACCURACY ALGORITHM VARIATION

As shown in Fig. 3, the proposed algorithm is two orders of magnitude faster than the existing iterative ones. However, both Newton–Raphson and gradient descent converge to a slightly lower value of the cost function resulting in a little better accuracy. In this section, a variation of the introduced algorithm is presented, as a balance between computational

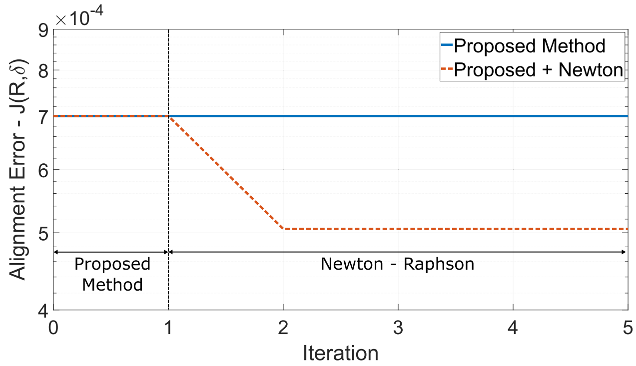

(a)

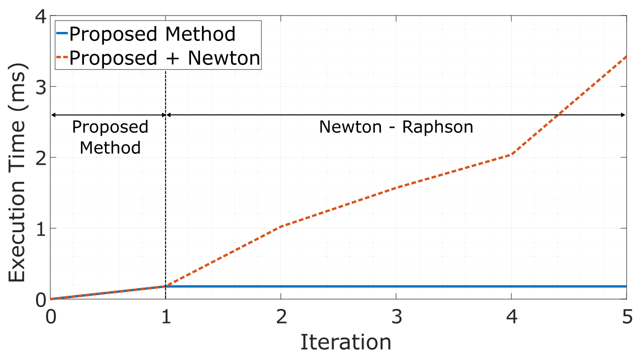

(b)

Fig. 4. Performance comparison between the proposed algorithm and its combination with the Newton–Raphson method. (a) Alignment error of the proposed algorithm compared with the alignment error of its combination with the Newton–Raphson method parameterized on their iteration step. (b) Execution time of the proposed algorithm compared with the execution time of its combination with the Newton–Raphson method parameterized on their iteration step.

efficiency and accuracy. More specifically, we run the proposed algorithm and then use the resulting matrix $\hat{R}$ and inclination angle δ as initial estimates for the Newton–Raphson method. As shown in Fig. 4, when the Newton–Raphson is initialized using the results of the proposed algorithm, it converges after just one iteration and about 1 ms.

We used the four recorded data sets of Section IV-A and run the proposed algorithm's variation 100 times for every data set. The MET for the 400 runs was about 1.15 ms. Although it is about four times slower than the proposed algorithm 1, it is still up to 100 times faster than the existing iterative algorithms based on the Newton–Raphson and gradient descent methods. Using the simulated measurements mentioned in Section IV-B, we evaluated the algorithm's residual alignment error matrix E. The results shown in Table III demonstrate the increased accuracy of the combination of the two methods compared with the proposed algorithm alone.

VI. Conclusion

A single-step method for aligning the coordinate frames of a three-axis accelerometer and a three-axis magnetometer was presented. The proposed method exploits the magnetic inclination to provide a closed-form expression for both the axes alignment matrix and the inclination angle. Using experimental results, we demonstrated that the proposed algorithm is about two orders of magnitude faster than similar algorithms using the gradient descent or the Newton–Raphson methods. Experimental data demonstrated that although the proposed method excels in computational efficiency, both Newton–Raphson and gradient descent-based algorithms provided slightly increased accuracy. As a balance between computational efficiency and accuracy, we also proposed a combination of the introduced method with the Newton–Raphson one. Although it is four times slower than the introduced method, this variation provides increased accuracy and up to 100 times less execution time than the Newton–Raphson alone.

Appendix
Alternative Ways To Derive s_δ

An alternate way to derive s_δ, instead of using (19), is presented. This approach is also based on the fact that when perfect measurements are considered, it is $R \in SO(3)$. Using this fact, we search for s_δ that minimizes the distance of $R = s_\delta H$ from orthogonality. To this purpose, we define the cost function

$$J(s_\delta) = \|R^T R - I\|_F^2 \tag{25}$$

and form the following optimization problem to calculate s_δ

$$\min_{s_\delta \in [-1,1]} \quad J(s_\delta). \tag{26}$$

Using the definition of the Frobenius norm, we write (25) as

$$J(s_\delta) = \operatorname{tr}\big((R^T R - I)^T (R^T R - I)\big). \tag{27}$$

Replacing (14) in (27), a solution of (26) is given in a closed form in the following by solving $dJ(s_\delta)/ds_\delta = 0$,

$$s_\delta = \operatorname{sgn}(\det(H))\sqrt{\frac{\operatorname{tr}(H^T H)}{\operatorname{tr}(H^T H H^T H)}} \tag{28}$$

where the sign of s_δ has been determined using (18). Using an SVD of H, i.e., $H = U\Sigma V^T$, where $U, V \in O(3)$ and Σ is the diagonal matrix $\Sigma = \operatorname{diag}(\sigma_1, \sigma_2, \sigma_3)$, with $\sigma_1 \geq \sigma_2 \geq \sigma_3 > 0$, we rewrite (28) in for form

$$s_\delta = \operatorname{sgn}(\det(H))\sqrt{\frac{\sigma_1^2 + \sigma_2^2 + \sigma_3^2}{\sigma_1^4 + \sigma_2^4 + \sigma_3^4}}. \tag{29}$$

References

[1] H. Guo, M. Uradzinski, H. Yin, and M. Yu, "Indoor positioning based on foot-mounted IMU," *Bull. Polish Acad. Sci. Tech. Sci.*, vol. 63, no. 3, pp. 629–634, Sep. 2015.

[2] J.-S. Hu and K.-C. Sun, "A robust orientation estimation algorithm using MARG sensors," *IEEE Trans. Instrum. Meas.*, vol. 64, no. 3, pp. 815–822, Mar. 2015.

[3] R. Zhu and Z. Zhou, "A real-time articulated human motion tracking using tri-axis Inertial/Magnetic sensors package," *IEEE Trans. Neural Syst. Rehabil. Eng.*, vol. 12, no. 2, pp. 295–302, Jun. 2004.

[4] K. Papafotis and P. P. Sotiriadis, "MAG. IC AL.–A unified methodology for magnetic and inertial sensors calibration and alignment," *IEEE Sensors J.*, vol. 19, no. 18, pp. 8241–8251, Sep. 2019.

[5] Y. Wu, D. Zou, P. Liu, and W. Yu, "Dynamic magnetometer calibration and alignment to inertial sensors by Kalman filtering," *IEEE Trans. Control Syst. Technol.*, vol. 26, no. 2, pp. 716–723, Mar. 2018.

[6] M. Kok, J. D. Hol, T. B. Schön, F. Gustafsson, and H. Luinge, "Calibration of a magnetometer in combination with inertial sensors," in *Proc. 15th Int. Conf. Inf. Fusion*, Singapore, Jul. 2012, pp. 787–793.

[7] M. Kok and T. B. Schön, "Maximum likelihood calibration of a magnetometer using inertial sensors," *IFAC Proc. Volumes*, vol. 47, no. 3, pp. 92–97, 2014. [Online]. Available: http://www.sciencedirect.com/science/article/pii/S1474667016415983

[8] J. Metge, R. Mégret, A. Giremus, Y. Berthoumieu, and T. Décamps, "Calibration of an inertial-magnetic measurement unit without external equipment, in the presence of dynamic magnetic disturbances," *Meas. Sci. Technol.*, vol. 25, no. 12, Dec. 2014, Art. no. 125106. [Online]. Available: http://stacks.iop.org/0957-0233/25/i=12/a=125106

[9] M. V. Gheorghe, "Calibration for tilt-compensated electronic compasses with alignment between the magnetometer and accelerometer sensor reference frames," in *Proc. IEEE Int. Instrum. Meas. Technol. Conf. (I2MTC)*, May 2017, pp. 1–6.

[10] X. Li and Z. Li, "A new calibration method for tri-axial field sensors in strap-down navigation systems," *Meas. Sci. Technol.*, vol. 23, no. 10, Sep. 2012, Art. no. 105105.

[11] K. Papafotis and P. P. Sotiriadis, "Accelerometer and magnetometer joint calibration and axes alignment," *Technologies*, vol. 8, no. 1, p. 11, Jan. 2020.

[12] R. A. Horn and C. R. Johnson, *Matrix Analysis*. Cambridge, U.K.: Cambridge Univ. Press, 2013.

[13] G. Strang, *Linear Algebra and Its Applications*. Boston, MA, USA: Cengage Learning, 2007.

[14] P. H. Schönemann, "A generalized solution of the orthogonal procrustes problem," *Psychometrika*, vol. 31, no. 1, pp. 1–10, Mar. 1966.

Paul P. Sotiriadis (Senior Member, IEEE) received the Diploma degree in electrical and computer engineering from the Electrical and Computer Engineering Department, National Technical University of Athens, Athens, Greece, in 1994, the M.S. degree in electrical engineering from Stanford University, Stanford, CA, USA, in 1996, and the Ph.D. degree in electrical engineering and computer science from the Massachusetts Institute of Technology, Cambridge, MA, USA, in 2002.

In 2002, he joined Johns Hopkins University, Baltimore, MD, USA, as an Assistant Professor of electrical and computer engineering. In 2012, he joined the faculty of the Electrical and Computer Engineering Department, National Technical University of Athens. He is currently a Faculty Member with the Electrical and Computer Engineering Department, National Technical University of Athens, the Director of the Electronics Laboratory, National Technical University of Athens, and a member of the governing board of the Hellenic Space Center (National space center of Greece). He has authored or coauthored more than 150 research publications, most of them in IEEE journals and conferences, holds one patent, and has contributed chapters to technical books. His research interests include design, optimization, and mathematical modeling of analog and mixed-signal circuits, RF and microwave circuits, advanced frequency synthesis, biomedical instrumentation, and interconnect networks in deep-submicrometer technologies. He has led several projects in these fields funded by U.S. organizations and has collaborations with industry and national laboratories.

Dr. Sotiriadis has received several awards, including the 2012 Guillemin-Cauer Award from the IEEE Circuits and Systems Society, the Best Paper Award at the IEEE International Symposium on Circuits and Systems in 2007, the Best Paper Award at the IEEE International Frequency Control Symposium in 2012, and the Best Paper Award at the IEEE International Conference on Modern Circuits and Systems Technologies in 2019. He is also an Associate Editor of the IEEE SENSORS JOURNAL. He has served as an Associate Editor for the IEEE TRANSACTIONS ON CIRCUITS AND SYSTEMS—I: REGULAR PAPERS from 2016 to 2020 and the IEEE TRANSACTIONS ON CIRCUITS AND SYSTEMS—II: EXPRESS BRIEFS from 2005 to 2010. He has been a member of the technical committee of many conferences. He is a regular reviewer for many IEEE transactions and conferences and serves on proposal review panels.

Konstantinos Papafotis (Graduate Student Member, IEEE) received the Diploma degree in electrical and computer engineering from the National Technical University of Athens, Athens, Greece, in 2015, where he is currently pursuing the Ph.D. degree under the supervision of Prof. P. P. Sotiriadis.

He is currently a teaching assistant in several undergraduate courses and acts as an advisor for several diploma theses. He is the author of several conference papers and journal articles. His main research interests include inertial navigation, embedded systems, and wireless sensor systems.

Mr. Papafotis received the Best Paper Award at the IEEE International Conference on Modern Circuits and Systems Technologies in 2019. He is a regular reviewer for many IEEE publications.